

## Data-driven respiratory motion tracking and compensation in CZT cameras: A comprehensive analysis of phantom and human images

Chi-Lun Ko, MD,<sup>a,b</sup> Yen-Wen Wu, MD, PhD,<sup>b,c,d,e</sup> Mei-Fang Cheng, MD,<sup>b</sup> Ruoh-Fang Yen, MD, PhD,<sup>b</sup> Wen-Chau Wu, PhD,<sup>f</sup> and Kai-Yuan Tzen, MD<sup>b</sup>

<sup>a</sup> Department of Nuclear Medicine, National Taiwan University Hospital Yun-Lin Branch, Douliou City, Yunlin County, Taiwan

<sup>b</sup> Department of Nuclear Medicine, National Taiwan University Hospital and National Taiwan University College of Medicine, Taipei, Taiwan

<sup>c</sup> Division of Cardiology, Department of Internal Medicine, National Taiwan University Hospital and National Taiwan University College of Medicine, Taipei, Taiwan

<sup>d</sup> Department of Nuclear Medicine and Cardiology Division of Cardiovascular Medical Center, Far Eastern Memorial Hospital, New Taipei City, Taiwan

<sup>e</sup> National Yang-Ming University School of Medicine, Taipei, Taiwan

<sup>f</sup> Graduate Institute of Oncology, National Taiwan University, Taipei, Taiwan

Received Jan 13, 2014; accepted Jul 10, 2014

doi:10.1007/s12350-014-9963-8

**Background.** This study described a method for tracking and compensating respiratory motion in cadmium-zinc-telluride (CZT) cameras. We evaluated motion effects on myocardial perfusion imaging and assessed the usefulness of motion compensation in phantom and clinical studies.

**Methods.** SPECT studies were obtained from an oscillating heart phantom and 552 patients using CZT cameras with list-mode acquisition. Images were reformatted in 500-ms frames, and the activity centroid was calculated as respiratory signal. The myocardial perfusion, left ventricular (LV) wall thickness, and LV volume were assessed before and after the motion compensation technique.

**Results.** In phantom studies, we documented only minimal bias between simulated and measured shifts. Significantly reduced tracer activity, increased wall thickness and decreased volume in scans with 15 mm or more axial shifts were noted. In clinical studies, there was a higher prevalence of significant motion after treadmill exercise. The motion compensation technique could successfully compensate those motion artifacts.

**Conclusion.** The described method allows for tracking and compensating respiratory motion in CZT cameras. Significant respiratory motion is still not uncommon using CZT cameras, especially in patients who underwent treadmill tests. Motion blurring can be compensated using image processing techniques and image quality could be significantly improved. (J Nucl Cardiol 2015;22:308–18.)

**Key Words:** List mode • myocardial perfusion imaging (MPI) • cadmium-zinc-telluride (CZT) • respiratory motion • motion compensation

## INTRODUCTION

The myocardium is constantly moving during single photon emission computerized tomography (SPECT) myocardial perfusion imaging (MPI). This movement is mainly due to patient motion, respiration, myocardial contraction, and upward creeping. These motions may blur projection images, reduce image resolution, and cause image artifacts.<sup>1-5</sup>

Previous investigations have reported that cardiac movements during respiration are dominated by cranial-caudal motion, and its excursion distance ranges from 4 to 18 mm using cardiac magnetic resonance imaging<sup>6</sup> and cardiac positron emission tomography (PET).<sup>7</sup> Several motion-tracking techniques, including external tracking systems and data-driven analytical methods, have attempted to measure respiratory motion. External tracking systems rely on additional equipment to generate respiratory signals, such as electrodes,<sup>5</sup> video tracking systems,<sup>8</sup> and elastic straps,<sup>9</sup> which may not correlate well with internal organ motion. Analytical methods, such as tracking activity center-of-mass (COM),<sup>10-13</sup> calculating cross-correlation functions,<sup>14</sup> and a posteriori gating for PET based on time-activity curve,<sup>15,16</sup> require only emission data from scanners. However, their utility is limited for conventional SPECT due to discrepant projections and insufficient count rates.<sup>10</sup>

The recently introduced cardiac SPECT camera utilizes solid-state cadmium-zinc-telluride (CZT) detectors.<sup>17</sup> The miniature detector and multi-pinhole collimator design enables simultaneous acquisition of angular data in 19 projections without detector rotation, which resembles PET. This may reduce the inconsistency between different angular projections owing to patient motion. The efficient collimation system provided a fivefold-increased myocardial count rate and allowed a shortened scan time,<sup>18,19</sup> which might theoretically reduce patient movements. Nevertheless, the respiratory motion remained despite shortened imaging time. In addition, improved image spatial resolution of the system may augment a motion-dependent partial-volume effect.<sup>20</sup>

In this study, we designed an algorithm to track respiratory motion and to compensate the three-dimensional (3D) motion in CZT cameras without auxiliary equipment. We validated this proposed technique on a physically oscillating cardiac phantom, and further applied to patient studies.

## MATERIALS AND METHODS

### Study Design and Subjects

This study included three parts. First, we designed a data-driven algorithm for respiratory motion tracking and motion

compensation. Second, we validated this method by using a physically oscillating cardiac phantom, mimicking the respiratory motion, to evaluate the motion artifacts and the performance of motion compensation technique. Finally, we applied this tracking and compensation methods in human images, evaluated the prevalence of respiratory motion of clinical significance, and assessed the performance of motion compensation technique.

### The CZT Camera and Image Processing

All SPECT images were acquired using a CZT gamma camera (Discovery NM530c, GE Medical System Israel, Tirat Hacarmel, Israel)<sup>17</sup> which was equipped with 19 pinhole collimators and 19 CZT detectors that covered the heart from right anterior oblique to left posterior oblique views. Each detector contained  $32 \times 32$  pixilated ( $2.46 \times 2.46$  mm) CZT elements. A built-in electrocardiography monitor was used for collecting cardiac gating signals.

Two energy windows were set asymmetrically ( $-14\%$  to  $+23\%$ ) at 70 keV and symmetrically ( $-9\%$  to  $+9\%$ ) at 167 keV for <sup>201</sup>Tl according to the factory settings. Data were stored in both list mode and frame mode. Images were transferred in DICOM format and processed by a built-in application (Myovation for Alcyone, GE Healthcare) on the Xeleris™ workstation. SPECT data was resampled along the short, vertical long, and horizontal long axes for display.

### The Respiratory Motion Tracking Algorithm and Quality Control

We developed an in-house program to extract the list-mode data from the dataset. Events within the energy window described previously were divided in 500-ms frames. We back-projected each event to 19 object planes, which were, respectively, parallel to the corresponding image planes, the surface of 19 CZT detectors, and intersected at the common focal point of multi-pinhole system.

After back-projection, our in-house program automatically selected a spherical volume of interest (VOI) enclosing the heart (Figure 1A) with an option of manual adjustment in some cases with prominent extracardiac activities. We calculated the axial COM for each frame by averaging the axial positions of back-projected events in the VOI. The calculation resulted in an axial motion curve of heart. Because the sampling frequency is far below the sampling frequency for cardiac contraction, no low-pass filter was applied. In addition, we determined the respiratory rate by recognizing the frequency component with maximum amplitude after fast Fourier transform.

To assess the motion tracking quality of clinical scans, we calculated the signal-to-noise ratio (SNR) of detected motion curve. We divided mean square amplitude of normalized axial motion curve within the VOI (signal) by mean square amplitude of the curve outside the VOI (noise). We proposed the SNR of more than 2 as good tracking quality in the current study, and only scans with  $SNR > 2$  were included for imaging analysis.

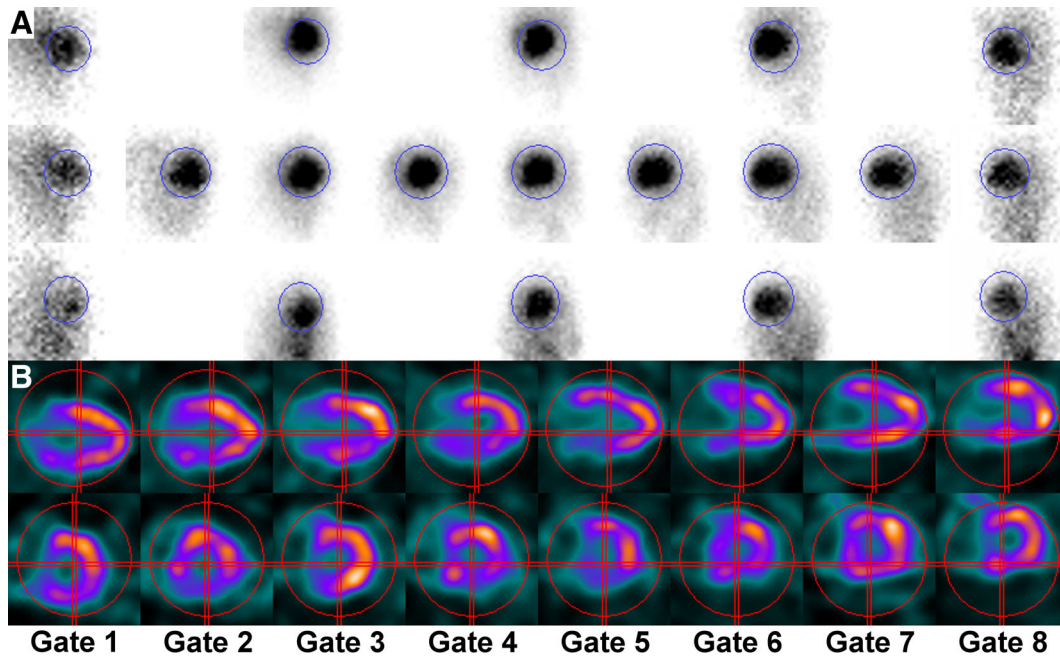


**Figure 1.** An example of automatic VOI selection. The VOI enclosing the heart was transformed on 19 projection images (A) and was displayed on eight respiratory-gated SPECT images (B) in vertical long-axis view (*upper panel*) and short-axis view (*lower panel*).

### Measurement of 3D Displacements in Respiratory-Gated Images

We sorted those 500-ms frames according to calculated axial COM; the sorted frames were divided into eight equal-sized respiratory gates (gate 1 to gate 8, representing end-inspiration to end-expiration) with each gate containing 12.5% of total frames; and respiratory-gated SPECT images were reconstructed (Figure 1B). The SPECT images within the cardiac VOI mentioned previously were iteratively shifted in three axes against the end-inspiration image (gate 1). The correlation coefficients reached their maximum value when the displacement between these two images was completely compensated.<sup>12</sup> The maximum displacement in three axes was recognized as measured motion. The calculation was done by our in-house software fully automatically with tri-cubic interpolation and coarse-to-fine approach.<sup>21</sup> The finest adjustment during calculation was about 0.1 mm.

### Motion Compensation and Image Reconstruction

In order to compensate for the motion on this multi-pinhole system, we designed a reconstruction program which incorporated the motion compensation process into the MAPEM algorithm. A similar reconstruction process has been described in conventional SPECT camera with parallel-hole collimator.<sup>22</sup> For each gated set ( $k = 1-8$ ), we modeled a new system matrix ( $a^k$ ) which shifted the reconstruction coordinates according to the 3D displacement measured in previous step

$$x_j^{\text{next}} = x_j^{\text{current}} \frac{1}{\sum_k \sum_i a_{ij}^k + \beta \frac{\partial U}{\partial x_j}} \sum_k \sum_i a_{ij}^k \frac{p_i^k}{\sum_j a_{ij}^k x_j^{\text{current}}},$$

where  $x^{\text{next}}$  and  $x^{\text{current}}$  denote both the next and current estimations of SPECT images,  $p^k$  denotes the projection image of gate  $k$ ,  $\beta$  denotes the adjustable factor for the prior, and  $\frac{\partial U}{\partial x_j}$  denotes the partial derivative of median root prior energy function. We used Green's one-step-late algorithm<sup>23</sup> with the median root prior<sup>24</sup> to account for noise regulation. The SPECT image was then reconstructed with 70 iterations. In comparison, we reconstructed the non-compensated SPECT images with the same algorithm and the same parameters, except those system matrices were not modified for motion.

### The Phantom Study

In order to validate this motion tracking and respective motion compensation algorithm, we designed a moving heart phantom by placing a Cardiac Insert<sup>TM</sup> phantom (Data Spectrum Corporation, Hillsborough, NC, USA) on an in-house moving plate which was controlled by a microcontroller with a programmed motion frequency and distance in sinusoidal oscillation along the cranial-caudal axis, mimicking respiratory motion (Figure 2A).<sup>9</sup> A dose of 7.4 MBq <sup>201</sup>Tl was loaded into the Cardiac Insert and the inner chamber was filled with water.

A motionless phantom acquisition was obtained for reference and followed by acquisition of 2.5-25 mm axial

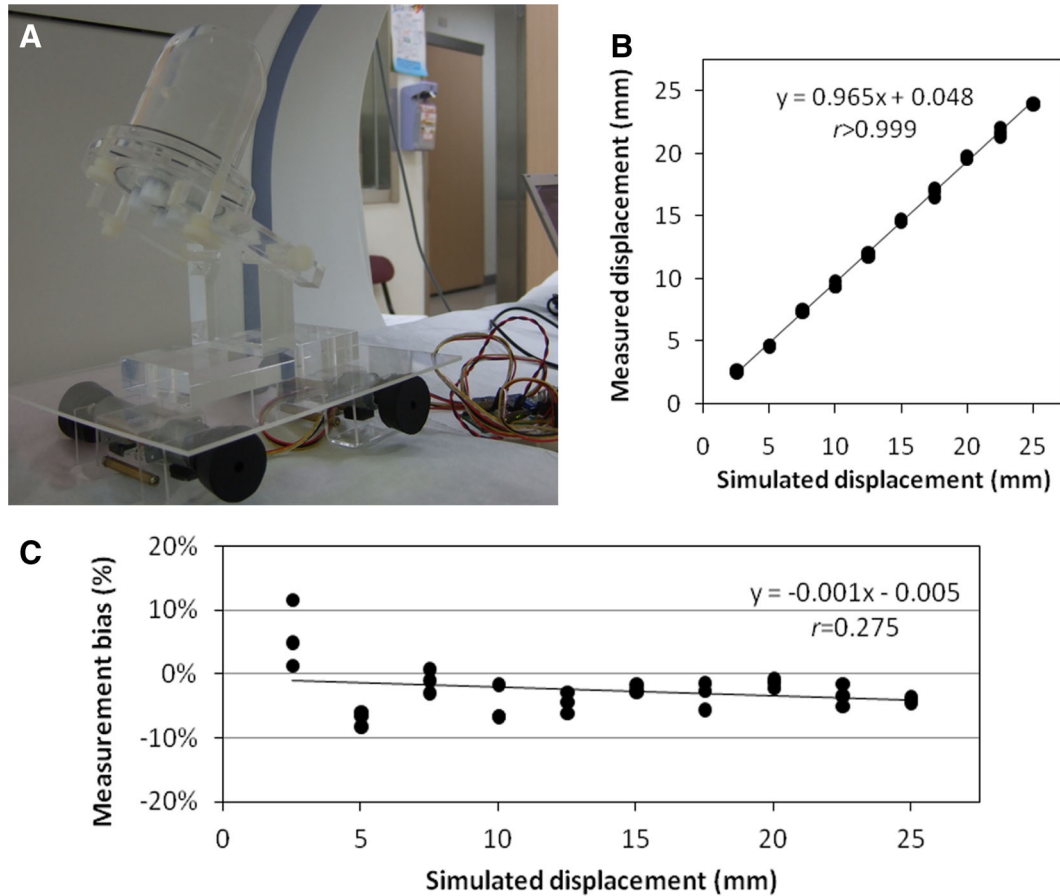


**Figure 2.** Cardiac Insert™ phantom was placed on top of in-house moving plate, which oscillated along cranial-caudal direction, mimicking respiratory motion (A). Simulated and measured axial displacements showed excellent correlation (B) with minimal bias (C). There is no significant correlation between bias and simulated displacement ( $P = .141$ ).

shifts (2.5-mm interval) with a frequency of 12 times per minute. The acquisition time was 120 seconds for each scan. The algorithm was applied to detect and to compensate the artificial motion. Phantom studies were repeated three times.

### Clinical Study Population and Study Protocol

Patients underwent stress and rest  $^{201}\text{Tl}$  MPI in the Department of Nuclear Medicine, National Taiwan University Hospital between November 1st, 2011 and November 30th, 2011 were retrospectively recruited for image analysis. Their age, gender, height, weight, body mass index (BMI), and risk factors were obtained from the medical records. The study was approved by the institutional review board of National Taiwan University Hospital.

All patients received standardized stress protocols in our institution.<sup>25</sup> In brief, 1 day stress/rest protocols were performed using either standardized symptom-limited Bruce treadmill or vasodilator dipyridamole ( $0.14 \text{ mg}\cdot\text{kg}^{-1}\cdot\text{minute}^{-1}$  over 4 minutes) protocols. A dose of  $111 \text{ MBq } ^{201}\text{Tl}$  was given at either peak stress of the treadmill test or three minutes after

completion of dipyridamole infusion. Those patients with severe hypoperfusion in post-stress images received additional  $37 \text{ MBq}$  of  $^{201}\text{Tl}$ . Imaging acquisition started at 5 minutes and 4 h later in the supine position with the hands raised above head. Acquisitions were preceded by automatic heart positioning in the optimal area, or “quality field of view,” using real-time preview displays. All acquisitions were electrocardiographically gated. The imaging time was 180 seconds post-stress and 240 seconds in redistribution scans; these may be prolonged if there is an arrhythmia.

### Image Analysis

Images were analyzed with a commercially available software package (QPS/QGS; Cedars-Sinai Medical Center, Los Angeles, CA, USA). Automatic processing was performed in all cases, with the option of manual correction in cases of inadequate anatomic delineation. In order to evaluate the motion compensation effects, we assessed (1) the normalized perfusion of mid-anterior wall (i.e., segment 7) on bull’s eye maps and (2) the left ventricular (LV) chamber volume from the non-gated images in the pre- and post-compensation scans

by using QPS analysis. We additionally measured (3) the mid-anterior wall thickness in our in-house software by calculating the mean of the full width at the half maximum Gaussian profile taken on three consecutive mid-ventricular short-axis slices. (4) In human image studies, automated quantification of SPECT MPI using a 5-point system based on the severity of tracer uptake in a 20-segment model was obtained by QPS software. We defined the scans with “significant respiratory motion” as following: normalized perfusion difference of 10% or more in the mid-anterior wall comparing to the corrected images. Only clinical scans with good tracking quality were analyzed, and motion compensation technique would be applied in the clinical scans with “significant respiratory motion.”

### Statistical Analysis

All measured values were represented as mean  $\pm$  SD. Comparisons between continuous and categorical variables were made using a Student's *t* test and  $\chi^2$  analysis, respectively. Correlation between continuous variables was assessed by Pearson tests valued as *r* = 0, poor; 0.01-0.20, slight; 0.21-0.40, fair; 0.41-0.60, moderate; 0.61-0.80, good; and 0.81-1.00, excellent. Associations between quantitative imaging analysis and clinical parameters were first analyzed by simple regression analysis and subsequently by stepwise multivariable analysis. All analyses were performed using STATA version 10.0 (StataCorp LP, College Station, TX, USA) statistical software. Each statistical test was two-sided, and a *P* value of  $<.05$  was considered statistically significant.

## RESULTS

### Phantom Study: Validation of the Tracking Algorithm

In motionless acquisition, the measured motion was  $0.05 \pm 0.05$ ,  $0.11 \pm 0.14$ , and  $0.15 \pm 0.04$  mm, respectively for left-right, ventral-dorsal, and cranial-caudal axes. In motion phantom scans (Figure 2B, C), there was an excellent correlation between the simulated and measured axial shifts ( $r > 0.999$ ,  $P < .001$ ). Our algorithm overestimated the shift by  $6\% \pm 5\%$  in 2.5 mm simulated axial motion while underestimated by  $3\% \pm 2\%$  with 5 mm or more simulated axial motion. There was no significant correlation between the amplitude of simulated motion and resulted differences ( $r = 0.28$ ,  $P = .14$ ).

### Phantom Study: Evaluation of the Effects of Axial Motion and Compensation Technique

The effects of both axial motion and motion compensation on perfusion imaging with different shifting distances are shown in Figure 3A. Perfusion heterogeneity significantly increased in scans with

15 mm or more axial motion. The images were more uniform after motion compensation technique.

In the quantitative analysis, the normalized perfusion activity of mid-anterior segment significantly decreased in scans with 10 mm or more axial motion ( $80.7\% \pm 2.5\%$  vs  $86.7\% \pm 2.1\%$ ,  $P = .035$ ). The mid-anterior wall of LV significantly increased in scans with 5 mm or more axial motion ( $14.5 \pm .2$  vs  $14.1 \pm 0.2$  mm,  $P = .044$ ). The LV chamber volume significantly decreased in scans with 12.5 mm or more axial motion ( $66 \pm 1$  vs  $70 \pm 1$  mL,  $P = .015$ ). All parameters could be successfully reversed after our motion compensation technique (Figure 3B).

### Patient Study: Evaluation of the Prevalence of Significant Respiratory Motion

A total of consecutive 564 patients were retrospectively reviewed and 12 studies were excluded due to missing datasets. Finally, 552 patients were recruited for analyses (159 treadmill and 393 dipyridamole tests, respectively). In general, there were more subjects of male, less diabetes, and younger age with similar BMI who underwent treadmill stress MPI. The clinical characteristics are summarized in Table 1.

The post-stress scans had a significantly higher count rate. Among 1,104 scans, there were 726 scans (66%) well tracked by our algorithm with SNR  $> 2$ . The proportion of good tracking quality is significantly higher in post-treadmill stress scans and significant lower in post-dipyridamole stress scans. The measured displacement along the cranial-caudal axis was more pronounced than either the ventral-dorsal or right-left axes (all  $P < .05$ ). The cranial-caudal displacement was significantly higher in treadmill group ( $12.0 \pm 4.3$  vs  $10.4 \pm 4.0$  mm,  $P < .001$ ). There was no significant difference between post-stress and rest scans. The results of the clinical scans are summarized in Table 2.

There were 34% of studies with SNR  $< 2$  which were excluded from final analysis because of relatively noisy projections. They may not be robust enough in low-count studies; however, the average axial displacement was  $6.6 \pm 2.5$  mm (0.6 to 16.3 mm) and only one scan had axial motion more than 15 mm.

According to the phantom experiment, an axial displacement of  $\geq 15$  mm could cause visually and quantitatively significant image deterioration. Therefore, 15 mm axial displacement was used as the threshold to select scans with significant motion. The prevalence was significantly higher in treadmill studies than dipyridamole for post-stress scans (14% vs 6%,  $P = .002$ ) but similar frequencies in the resting scans (11% vs 7%,  $P = .064$ ). The univariate regression analyses showed magnitude of motion was positively associated with the

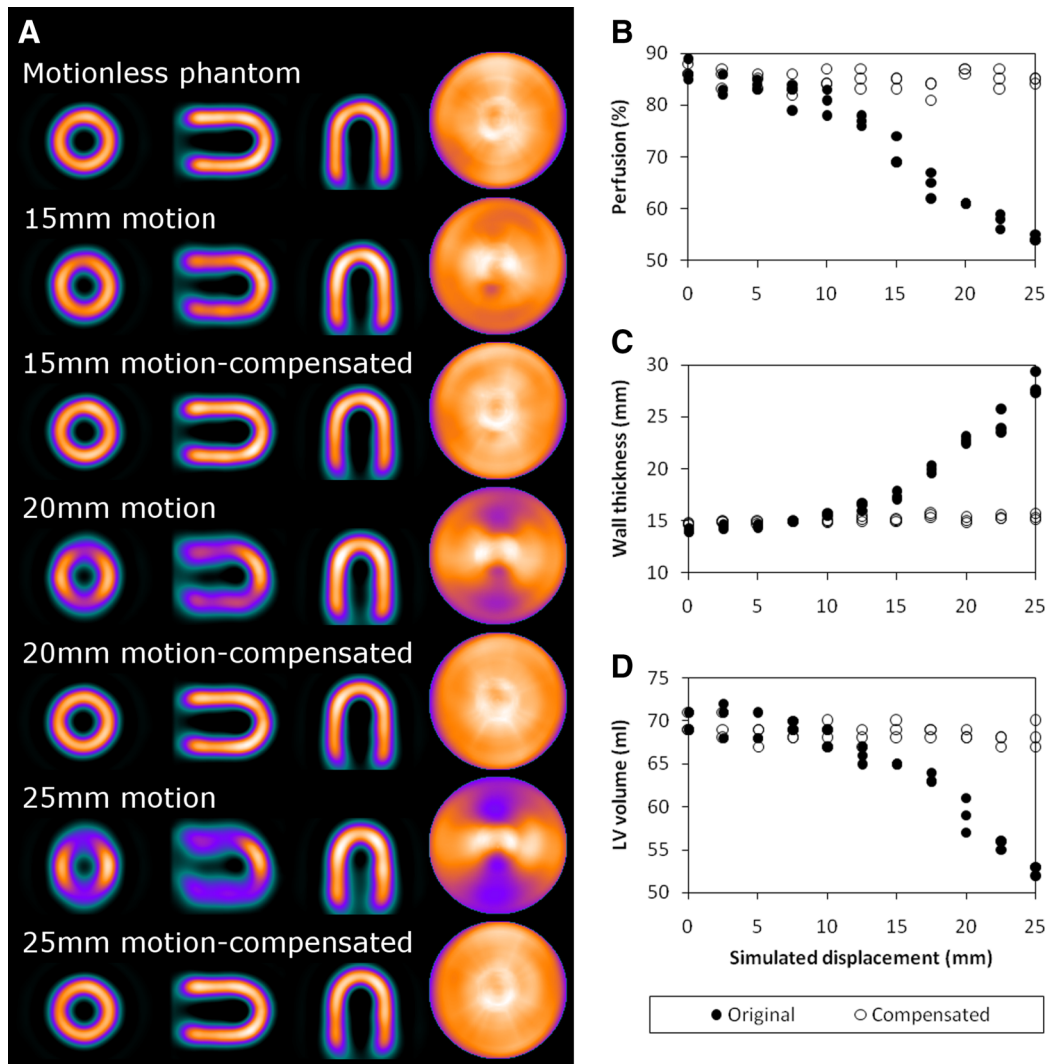


**Figure 3.** Effect of axial motion and motion compensation on phantom studies (A) and analyses of the effects of axial motion and motion compensation with regards to the normalized perfusion on mid-anterior segment (B), mid-anterior wall thickness (C), and non-gated LV chamber volume (D) in the phantom studies.

**Table 1.** Clinical characteristics of study population (n = 552)

Parameters	Treadmill (n = 159)	Dipyridamole (n = 393)	P value
Male gender (% , n)	73% (116)	55% (215)	<.001
Age (years)	60.1 ± 10.6	68.5 ± 11.0	<.001
Weight (kg)	69.1 ± 11.4	65.8 ± 12.1	.002
Height (cm)	165.2 ± 8.5	160.6 ± 8.1	<.001
Body mass index (kg·m <sup>-2</sup> )	25.2 ± 3.1	25.4 ± 4.0	.497
Hypertension (% , n)	66% (105)	68% (269)	.588
Diabetes (% , n)	25% (40)	38% (151)	.002
Dyslipidemia (% , n)	51% (81)	47% (185)	.412
Cigarette (% , n)	27% (43)	22% (92)	.380

**Table 2.** The motion effects in cardiac SPECT using CZT cameras (n = 552)

Parameters	Treadmill (n = 159)		Dipyridamole (n = 393)	
	Stress	Rest	Stress	Rest
Count rate (cps)	4,034 ± 978 <sup>a,b</sup>	2,784 ± 603 <sup>b</sup>	6,031 ± 1,409 <sup>a</sup>	3,891 ± 901
Heart rate (minute <sup>-1</sup> )	79 ± 10 <sup>a,b</sup>	71 ± 10	76 ± 13 <sup>a</sup>	72 ± 13
Respiratory rate (minute <sup>-1</sup> )	17.7 ± 5.8 <sup>b</sup>	16.5 ± 6.6	16.5 ± 6.2	17.3 ± 6.1
Signal to noise ratio	3.3 ± 1.9 <sup>a,b</sup>	2.6 ± 1.2 <sup>b</sup>	2.7 ± 1.7	2.8 ± 1.5
Good tracking quality (% , n)	82% (130) <sup>a,b</sup>	62% (98)	59% (232) <sup>a</sup>	68% (266)
Displacements				
Right-left (mm)	2.9 ± 1.8 <sup>b</sup>	2.5 ± 1.6	2.6 ± 1.4	2.4 ± 1.3
Ventral-dorsal (mm)	2.6 ± 1.8 <sup>b</sup>	2.9 ± 1.7 <sup>b</sup>	2.3 ± 1.3 <sup>a</sup>	2.5 ± 1.3
Cranial-caudal (mm)	12.3 ± 4.4 <sup>b</sup>	11.6 ± 4.1 <sup>b</sup>	10.5 ± 4.1	10.3 ± 3.8
Significant motion (% , n)	14% (23) <sup>b</sup>	11% (18)	6% (25)	7% (26)

<sup>a</sup>P < .05 between stress and rest scan.

<sup>b</sup>P < .05 between treadmill and dipyridamole group.

younger age, male gender, body weight, height, and treadmill stress type. Only treadmill mode, height and weight remained significant after the multivariate analysis (Table 3).

**Patient Study: Effects of Motion Compensation**

Among 1,104 scans, there were 93 (8.4%) scans with significant respiratory motion recognized for motion compensation. One scan was excluded due to insufficient tracking quality (SNR = 1.8). A final total of 92 SPECT image pairs were generated. An example of successful motion compensation was demonstrated in Figure 4. The differences of normalized perfusion before and after applying the motion compensation technique were demonstrated in the bull’s eye map (Figure 4A). There was significantly improved perfusion

in both anterior and inferior segments while decreased perfusion in anteroseptal and inferolateral segments were disclosed after motion compensation.

Quantitative analyses are shown in both Table 4 and Figure 5B-D. After motion compensation, the mid-anterior LV wall thickness (23.5 ± 2.6 vs 27.3 ± 4.7 mm) and summed scores (5.21 ± 5.79 vs 6.46 ± 5.80) significantly decreased; normalized perfusion activities of the mid-anterior segment (82.5% ± 8.7% vs 77.8% ± 8.7%) and the LV chamber volume (47.1 ± 19.9 vs 44.6 ± 19.4 mL) were significantly increased (all P < .001). All changes of these parameters were moderately correlated with the axial displacement (r = -0.59, -0.46, 0.41, and 0.52, respectively; all P < .001).

There were 12 patients with patent coronary arteries proven by the invasive coronary angiography. The original and motion-compensated images were quantitatively analyzed by QPS software and compared. Six of them (50%) had abnormal post-stress scans with total

**Table 3.** Univariate and multivariate regression with magnitude of motion

	Univariate regression		Multivariate regression	
	r	P value	β	P value
Age (years)	-0.148	.0001		
Male gender	0.222	<.0001		
Weight (kg)	0.274	<.0001	0.063	.0001
Height (cm)	0.274	<.0001	0.068	.0028
Stress type <sup>a</sup>	0.181	<.0001	1.029	.0018
Scan type <sup>b</sup>	0.063	.0896		
Imaging duration (seconds)	0.072	.0524		

<sup>a</sup>Treadmill (=1) or dipyridamole (=0).

<sup>b</sup>Stress (=1) or rest (=0).

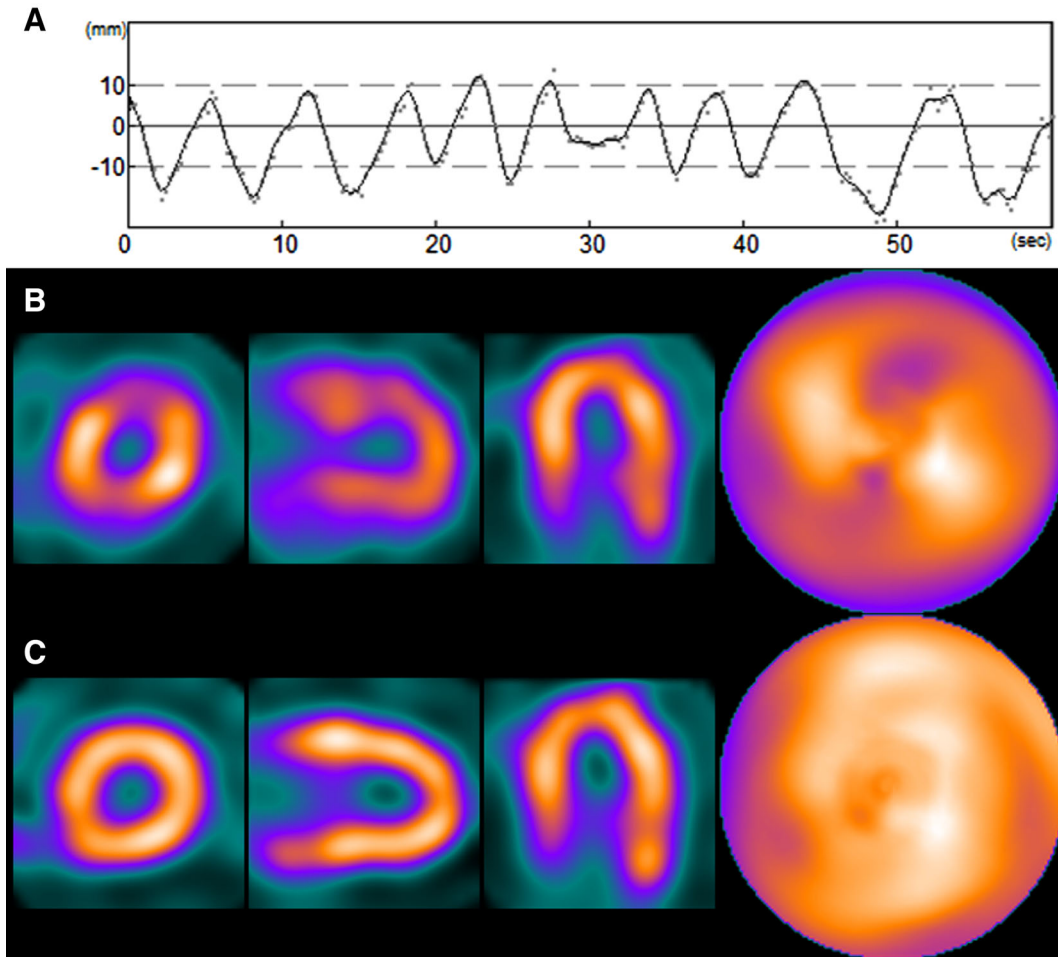


**Figure 4.** An example of motion compensation in a patient study. Our tracking program detected significant motion along cranial-caudal axis (A). The *gray dots* represent measured center of mass along cranial-caudal axis. The *black curve* represents post-filtered motion curve. Reconstructed SPECT images and polar map are displayed without motion compensation (B), and the same image reconstructed with motion compensation (C).

**Table 4.** SPECT image quantitative analysis with and without motion compensation

	<b>Pre-compensated</b>	<b>Post-compensated</b>	<b>P value</b>
Mid-anterior wall perfusion (%)	77.8 ± 8.7	82.5 ± 8.7	<.001
Mid-anterior wall thickness (mm)	27.3 ± 4.7	23.5 ± 2.6	<.001
Non-gated LV volume (mL)	44.6 ± 19.4	47.1 ± 19.9	<.001
Summed score	6.46 ± 5.80	5.21 ± 5.79	<.001

perfusion deficit  $\geq 5\%$ . The post-stress scan was completely normalized after the motion compensation technique in three cases, and their measured axial shifts were 14.51, 26.66, and 24.17 mm, respectively. The other nine scans remained unchanged after the motion compensation technique, and none had significant axial motion ( $9.1 \pm 4.2$  mm, range 1.3-13.9 mm). Although small case number, our data support that the motion

compensation technique should be considered in scans with 15 mm or more axial motion.

## DISCUSSION

Our study described a data-driven COM-based method to track and compensate respiratory motion in CZT cameras without auxiliary external device. We



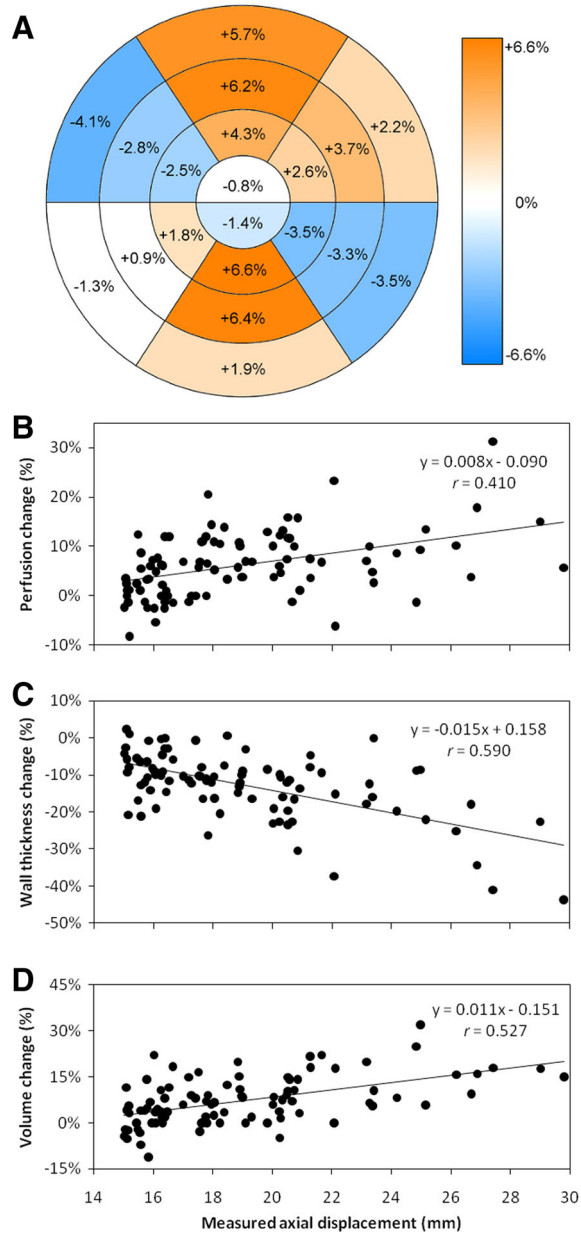


**Figure 5.** Averaged change of perfusion on 20-segment model of polar map after applying motion compensation technique on patient studies with significant axial motion (A). Perfusion of all segments were significantly changed, except for mid to basal inferoseptal and apical segments (the white blocks). And effects of motion compensation on normalized perfusion (B), mid-anterior wall thickness (C), and non-gated LV chamber volume (D) in patient studies.

validated the algorithm in both phantom and clinical studies. The axial motion due to respiration was not uncommon in clinical scans, especially after treadmill test. Significant respiratory motion may blur the perfusion image, and compensating for the motion resulted in significantly improved image quality in certain cases.

Until now, the utility of analytical motion tracking with conventional SPECT is still limited of use. The majority of published studies using center of mass-based analytical methods in SPECT were either based on phantom simulations,<sup>10,11,26,27</sup> or with aid from additional equipment for gating.<sup>28</sup> The projections are acquired sequentially by using conventional SPECT, thus respiratory-gated SPECT acquisition may result in inconsistency between projections and low-count rates may be a main barrier for utility of analytical methods for tracking patient motions by SPECT acquisition. The ultrafast cardiac CZT camera may overcome these problems by fivefold-increased count rate and simultaneous acquisition of 19 projection images.<sup>17-19</sup> Our algorithm was quite stable for the motionless phantom in three axes and the tiny disparity (<1 mm) could be due to the Poisson nature of emission data. Our phantom experiment also showed an excellent correlation between artificial and measured axial displacements with negligible deviation (<1 mm) which could be partly attributed to physical resolution of the moving plate.

Insufficient respiratory gating number may contribute to the underestimation of motion distance. Instead of using a threshold,<sup>10</sup> our algorithm adopted a different approach to deal with extracardiac soft tissue activities. We simply selected a VOI to enclose heart activity, thereby eliminating the disturbance from surrounding activity. With this selection, we can further differentiate motion signal from background soft tissue noise and establish a quality control mechanism for patient scans.

In the quantitative analysis of the phantom study, a considerable reduction of normalized perfusion activity in the mid-anterior segment in the scans with 10 mm or more simulated axial motion was noted. Kovalski et al<sup>20</sup> had reported similar observation in a phantom study using a conventional gamma camera. Our study demonstrated that significant motion reduced perfusion activity and LV chamber volume, and increased wall thickness. Our proposed technique may compensate the motion-dependent partial-volume effect, resulting improved imaging quality.

Different ranges of respiratory motion distance have been reported. Kovalski et al<sup>20,28</sup> reported  $7.0 \pm 2.6$  mm (2.7-17.3 mm) of respiratory motion in <sup>99m</sup>Tc sestamibi SPECT. Meanwhile, Buther et al<sup>12</sup> reported their scans had  $9.4 \pm 4.5$  mm of mean displacement of LV wall in <sup>18</sup>F-FDG PET. Livieratos et al<sup>7</sup> reported  $8.5 \pm 4.8$  mm (4.5-16.5 mm) of centroid excursion in the in vivo <sup>15</sup>O PET scans. In our clinical studies, the mean axial shift was  $10.9 \pm 4.1$  mm (3.2-29.8 mm), higher value could be due to lower myocardial count rate of <sup>201</sup>Tl.

In our clinical study, the body weight and height of subjects positively correlated with larger respiratory

amplitude in cranial-caudal direction, as previously reported by ultrasonography.<sup>29,30</sup> Although longer acquisition time is anticipated to increase the patients' motion; multivariate analysis showed no association between acquisition time and motion. A possible explanation was that the mean scan time was only  $4.4 \pm .8$  minutes (ranged from 3.0 to 10.0 minutes) by using CZT cameras.

Our clinical study showed the treadmill stress mode was the most important contributor of significant respiratory motion; a possible explanation was deep breathing after vigorous exertion. Studies with  $^{201}\text{Tl}$  are expected higher prevalence than  $^{99\text{m}}\text{Tc}$  tracers partly due to immediate acquisition after stress. By reviewing the 3D motion curve, we found that most non-periodic shifts originated from the initial deep breathing or "upward creep of the heart" (usually along the cranial-caudal axis).<sup>3</sup> However, those abrupt shifts contributed only a small portion to the displacement; and they could be removed from list-mode data or reduced by quiet bed rest on the imaging table before acquisition.<sup>31</sup> On the contrary, respiratory motion is cyclic and has greater effect on downgrading the quality of SPECT. Buechel et al<sup>32,33</sup> established a protocol for real-time breath-hold triggering of the MPI on the CZT SPECT camera, resulting significant differences of the left ventricular volume, stroke volume, and wall motion measurements between respiration triggering and normal breath studies. However, repeated breath-holding requires patients' cooperation and is time-consuming. The depth of breath-holding may be inconsistent between triggers which could even cause motion artifacts. Therefore, our method provides a simple and reliable solution to track respiratory motion and to correct motion artifacts.

### LIMITATIONS

The first is the lack of comparison with an external motion tracking system in the current study. Second, we validated our motion tracking system with a moving heart phantom and applied to the clinical scans, but only in cranial-caudal axis. The gap between the clinical scenario exists because phantom studies could not represent the relative motion of heart and surrounding tissues. There is a commercial package for motion correction recently developed by the vendor of this camera; however, limited information and clinical validation of the software is published, and the software package is not available in our institute. Our proposed method could only detect and compensate rigid-body transformation. Finally,  $^{201}\text{Tl}$  rather  $^{99\text{m}}\text{Tc}$  tracer was used in this study, while it reflects the clinical practice in Taiwan.

### NEW KNOWLEDGE GAINED

Respiratory motion-related image blurring could be observed in MPI with CZT cameras despite shortened scan time and increased count rate. The movement is more prominent immediately after treadmill exercise. The motion artifacts could be compensated by using image processing technique, and image quality could be significantly improved.

### CONCLUSION

The technique reported in this study successfully track and compensate respiratory motion for CZT cameras in phantom and clinical studies. Axial movement generated by cyclic respiratory motion during MPI affects the imaging quality of perfusion images and LV functional parameters. Compensating technique should be applied for the scans with evident respiratory motion of clinical significance in certain cases. Further studies are warranted to confirm whether this technique could improve diagnostic accuracy and confidence in the clinical setting.

### Acknowledgments

*This study was partially supported by Grants NSC 100-2314-B-002-158 and NSC 101-2314-B-002-151-MY3 from National Science Council of Taiwan.*

### Disclosure

*None.*

### References

1. Agarwal V, DePuey EG. Myocardial perfusion SPECT horizontal motion artifact. *J Nucl Cardiol* 2014 [Epub ahead of print].
2. Koshino K, Watabe H, Enmi J, Hirano Y, Zeniya T, Hasegawa S, et al. Effects of patient movement on measurements of myocardial blood flow and viability in resting (15)O-water PET studies. *J Nucl Cardiol* 2012;19:524-33.
3. Friedman J, Van Train K, Maddahi J, Rozanski A, Prigent F, Bietendorf J, et al. "Upward creep" of the heart: A frequent source of false-positive reversible defects during thallium-201 stress-redistribution SPECT. *J Nucl Med* 1989;30:1718-22.
4. Cooper JA, Neumann PH, McCandless BK. Effect of patient motion on tomographic myocardial perfusion imaging. *J Nucl Med* 1992;33:1566-71.
5. Cho K, Kumiata S, Okada S, Kumazaki T. Development of respiratory gated myocardial SPECT system. *J Nucl Cardiol* 1999;6:20-8.
6. Wang Y, Riederer SJ, Ehman RL. Respiratory motion of the heart: Kinematics and the implications for the spatial resolution in coronary imaging. *Magn Reson Med* 1995;33:713-9.

7. Livieratos L, Rajappan K, Stegger L, Schafers K, Bailey DL, Camici PG. Respiratory gating of cardiac PET data in list-mode acquisition. *Eur J Nucl Med Mol Imaging* 2006;33:584-8.
8. Nehmeh SA, Erdi YE, Ling CC, Rosenzweig KE, Schoder H, Larson SM, et al. Effect of respiratory gating on quantifying PET images of lung cancer. *J Nucl Med* 2002;43:876-81.
9. Kovalski G, Israel O, Keidar Z, Frenkel A, Sachs J, Azhari H. Correction of heart motion due to respiration in clinical myocardial perfusion SPECT scans using respiratory gating. *J Nucl Med* 2007;48:630-6.
10. Bruyant PP, King MA, Pretorius PH. Correction of the respiratory motion of the heart by tracking of the center of mass of thresholded projections: A simulation study using the dynamic MCAT phantom. *IEEE Trans Nucl Sci* 2002;49:2159-66.
11. Feng B, Bruyant PP, Pretorius PH, Beach RD, Gifford HC, Dey J, et al. Estimation of the rigid-body motion from three-dimensional images using a generalized center-of-mass points approach. *IEEE Trans Nucl Sci* 2006;53:2712-8.
12. Buther F, Dawood M, Stegger L, Wubbeling F, Schafers M, Schober O, et al. List mode-driven cardiac and respiratory gating in PET. *J Nucl Med* 2009;50:674-81.
13. Bundschuh RA, Martinez-Moeller A, Essler M, Martinez MJ, Nekolla SG, Ziegler SI, et al. Postacquisition detection of tumor motion in the lung and upper abdomen using list-mode PET data: A feasibility study. *J Nucl Med* 2007;48:758-63.
14. Ueda Y, Kudomi S, Koike M, Oishi Y, Iwanaga H, Ueda K. Correction of liver displacement due to irregular respiration for SPECT images obtained using a multiple short-time acquisition with breath-holding technique. *Radiol Phys Technol* 2012;5:71-7.
15. Schleyer PJ, O'Doherty MJ, Barrington SF, Marsden PK. Retrospective data-driven respiratory gating for PET/CT. *Phys Med Biol* 2009;54:1935-50.
16. Kesner AL, Bundschuh RA, Detorie NC, Dahlbom M, Ziegler SI, Czernin J, et al. Respiratory gated PET derived in a fully automated manner from raw PET data. *IEEE Trans Nucl Sci* 2009;56:677-86.
17. Bocher M, Blevis IM, Tsukerman L, Shrem Y, Kovalski G, Volkov L. A fast cardiac gamma camera with dynamic SPECT capabilities: Design, system validation and future potential. *Eur J Nucl Med Mol Imaging* 2010;37:1887-902.
18. Buechel RR, Herzog BA, Husmann L, Burger IA, Pazhenkottil AP, Treyer V, et al. Ultrafast nuclear myocardial perfusion imaging on a new gamma camera with semiconductor detector technique: First clinical validation. *Eur J Nucl Med Mol Imaging* 2010;37:773-8.
19. Songy B, Lussato D, Guernou M, Queneau M, Geronazzo R. Comparison of myocardial perfusion imaging using thallium-201 between a new cadmium-zinc-telluride cardiac camera and a conventional SPECT camera. *Clin Nucl Med* 2011;36:776-80.
20. Kovalski G, Keidar Z, Frenkel A, Israel O, Azhari H. Correction for respiration artefacts in myocardial perfusion SPECT is more effective when reconstructions supporting collimator detector response compensation are applied. *J Nucl Cardiol* 2009;16:949-55.
21. Bergen J, Anandan P, Hanna K, Hingorani R. Hierarchical model-based motion estimation. In: Sandini G, editor. *Computer vision—ECCV'92*. Berlin: Springer; 1992. p. 237-52.
22. Dey J, King MA. Theoretical and numerical study of MLEM and OSEM reconstruction algorithms for motion correction in emission tomography. *IEEE Trans Nucl Sci* 2009;56:2739-49.
23. Green PJ. Bayesian reconstructions from emission tomography data using a modified EM algorithm. *IEEE Trans Med Imaging* 1990;9:84-93.
24. Sohlberg A, Kuikka JT, Ruotsalainen U. Pinhole single-photon emission tomography reconstruction based on median root prior. *Eur J Nucl Med Mol Imaging* 2003;30:217-21.
25. Wu YW, Yen RF, Chieng PU, Huang PJ. TI-201 myocardial SPECT in differentiation of ischemic from nonischemic dilated cardiomyopathy in patients with left ventricular dysfunction. *J Nucl Cardiol* 2003;10:369-74.
26. Dey J, Segars WP, Pretorius PH, Walvick RP, Bruyant PP, Dahlberg S, et al. Estimation and correction of cardiac respiratory motion in SPECT in the presence of limited-angle effects due to irregular respiration. *Med Phys* 2010;37:6453-65.
27. Beach RD, Depold H, Boening G, Bruyant PP, Feng B, Gifford HC, et al. An adaptive approach to decomposing patient-motion tracking data acquired during cardiac SPECT imaging. *IEEE Trans Nucl Sci* 2007;54:130-9.
28. Kovalski G, Keidar Z, Frenkel A, Sachs J, Attia S, Azhari H. Dual, "motion-frozen heart" combining respiration and contraction compensation in clinical myocardial perfusion SPECT imaging. *J Nucl Cardiol* 2009;16:396-404.
29. Boussuges A, Gole Y, Blanc P. Diaphragmatic motion studied by m-mode ultrasonography: Methods, reproducibility, and normal values. *Chest* 2009;135:391-400.
30. Harris RS, Giovannetti M, Kim BK. Normal ventilatory movement of the right hemidiaphragm studied by ultrasonography and pneumotachography. *Radiology* 1983;146:141-4.
31. Karacalioglu AO, Jata B, Kilic S, Arslan N, Ilgan S, Ozguven MA. A physiologic approach to decreasing upward creep of the heart during myocardial perfusion imaging. *J Nucl Med Technol* 2006;34:215-9.
32. Buechel RR, Pazhenkottil AP, Herzog BA, Husmann L, Nkoulou RN, Burger IA, et al. Real-time breath-hold triggering of myocardial perfusion imaging with a novel cadmium-zinc-telluride detector gamma camera. *Eur J Nucl Med Mol Imaging* 2010;37:1903-8.
33. Buechel RR, Husmann L, Pazhenkottil AP, Nkoulou R, Herzog BA, Burger IA, et al. Myocardial perfusion imaging with real-time respiratory triggering: Impact of inspiration breath-hold on left ventricular functional parameters. *J Nucl Cardiol* 2010;17:848-52.